PHILOSOPHICAL TRANSACTIONS OF THE ROYAL SOCIETY A

rsta.royalsocietypublishing.org

Research

Cite this article: Kurukuri S, Worswick MJ, Ghaffari Tari D, Mishra RK, Carter JT. 2014 Rate sensitivity and tension–compression asymmetry in AZ31B magnesium alloy sheet. *Phil. Trans. R. Soc. A* **372**: 20130216. http://dx.doi.org/10.1098/rsta.2013.0216

One contribution of 12 to a Theme Issue 'Shock and blast: celebrating the centenary of Bertram Hopkinson's seminal paper of 1914 (Part 1)'.

Subject Areas:
mechanical engineering

Keywords:
magnesium sheet, rate sensitivity, tension–compression asymmetry, anisotropy, material modelling, material characterization

Author for correspondence:
Srihari Kurukuri
e-mail: srihari.kurukuri@uwaterloo.ca

Royal Society Publishing

Rate sensitivity and tension–compression asymmetry in AZ31B magnesium alloy sheet

Srihari Kurukuri[1], Michael J. Worswick[1], Dariush Ghaffari Tari[1], Raja K. Mishra[2] and Jon T. Carter[2]

[1]Department of Mechanical and Mechatronics Engineering, University of Waterloo, 200 University Avenue West, Waterloo, Ontario N2L 3G1, Canada
[2]General Motors R&D, Chemical and Materials Systems Laboratory, Warren, MI 48090, USA

The constitutive response of a commercial magnesium alloy rolled sheet (AZ31B-O) is studied based on room temperature tensile and compressive tests at strain rates ranging from 10^{-3} to $10^{3}\,s^{-1}$. Because of its strong basal texture, this alloy exhibits a significant tension–compression asymmetry (strength differential) that is manifest further in terms of rather different strain rate sensitivity under tensile versus compressive loading. Under tensile loading, this alloy exhibits conventional positive strain rate sensitivity. Under compressive loading, the flow stress is initially rate insensitive until twinning is exhausted after which slip processes are activated, and conventional rate sensitivity is recovered. The material exhibits rather mild in-plane anisotropy in terms of strength, but strong transverse anisotropy (r-value), and a high degree of variation in the measured r-values along the different sheet orientations which is indicative of a higher degree of anisotropy than that observed based solely upon the variation in stresses. This rather complex behaviour is attributed to the strong basal texture, and the different deformation mechanisms being activated as the orientation and sign of applied loading are varied. A new constitutive equation is proposed to model the measured compressive behaviour that captures the rate sensitivity of the sigmoidal stress–strain response. The measured tensile stress–strain response is fit to the Zerilli–Armstrong hcp material model.

1. Introduction

Magnesium alloys being light in weight have potential applications in automotive and aerospace structural applications. Various potential automotive applications of wrought magnesium alloy sheet have been prototyped, but production implementation of sheet has been limited to a very low volume [1,2]. The issues which hinder widespread implementation of wrought magnesium alloys include the high cost of sheet, limited formability at room temperature, difficulty in joining to other materials and corrosion [2]. The limited formability is due to the hexagonal close-packed (hcp) structure of magnesium, which offers only a limited number of slip systems at room temperature owing to the strong basal crystallographic texture [3–5]. According to the von Mises–Taylor criterion, at least five independent slip systems are needed to accommodate an arbitrary homogeneous polycrystalline deformation. At room temperature, magnesium alloys have only four independent active slip systems. Furthermore, none of these active slip systems can accommodate deformation perpendicular to the crystallographic *c*-axis of the grain. Deformation at lower temperatures is therefore accommodated by activation of the twinning deformation mechanism [4,6–8]. Additional complications arise owing to the basal texture, and twinning deformation mode activated in compression deformation leads to strong tension–compression asymmetry in the mechanical response [3,4,7–10]. Wrought magnesium sheet exhibits very strong orientation-dependent rate sensitivity. For instance, Kurukuri *et al.* [11] characterized the response of ZEK100 rare-earth Mg alloy sheet over a range of strain rates (10^{-3} to $10^{3}\,s^{-1}$) and in different sheet orientations. It is reported that when pulling the sample in the rolling direction (RD), the rate sensitivity in ZEK100 is accompanied by significant changes in yield strength, but has a relatively mild effect on work hardening rate, such as many bcc alloys. When pulling ZEK100 sheet along the transverse direction (TD), the rate sensitivity is not accompanied by changes in early yield response, whereas the hardening rate increases significantly with strain rate as commonly observed for many fcc alloys. Kurukuri *et al.* [11] have pointed out that this orientation-dependent rate sensitivity of mechanical response of ZEK100 sheet is due to the initial crystallographic texture and the corresponding active deformation mechanisms.

Extensive research has been carried out on the plastic deformation behaviour of magnesium alloys, but most studies have focused on quasi-static loading conditions [12–14]. The high strain rate behaviour is of great interest to the automotive and aircraft sectors, because the dynamic response of components must be known to support design and simulation for severe loading conditions, such as crash or impact [15,16]. Mukai *et al.* [17] investigated the effect of grain size and observed that the ductility and tensile strength of the investigated magnesium alloy were increased at high rates of strain. El-Magd & Abouridouane [18] observed an increase in ductility for extruded AZ80 magnesium alloy under dynamic compressive loading. However, most of these high strain rate studies have concentrated on extruded magnesium alloys which usually have a different initial crystallographic texture compared with rolled sheets. Recently, the constitutive behaviour of commercial AZ31B rolled sheet at high strain rates was examined by Ulacia *et al.* [16], who observed that the flow stress and also elongation increase considerably at high strain rates when compared with quasi-static rates, resulting in an increase in energy absorption.

The compressive deformation of Mg alloy sheet at dynamic strain rates (order of $10^{3}\,s^{-1}$) has not been thoroughly investigated as yet. In particular, the effects of higher strain rate and sheet orientation on deformation mechanisms, yield strength and flow stress asymmetry and anisotropy are still unknown. The compression deformation studies carried out to date have dealt mostly with extruded and cast AZ and AM alloys [17,18]. It has been reported that ductility increases with increasing strain rate owing to an increase in the rate sensitivity. However, relatively few studies were performed considering the compressive mechanical behaviour of an AZ31 sheet at elevated strain rates. Tucker *et al.* [19] studied the anisotropic effects on the strain rate dependence by performing dynamic strain rate tests on 19 mm thick AZ31B sheet. The effect of temperature and sheet orientation on the compressive response was studied by Ulacia *et al.* [8] by performing compression tests on 3 mm thick AZ31B sheet at dynamic strain rates. Khan

et al. [7] studied the effect of temperature and sheet orientation on the tensile and compressive response of 2 mm thick automotive grade AZ31B sheet at quasi-static strain rates. Unfortunately, no experiments have been reported in which the same lot of magnesium sheet at thicknesses appropriate for automotive applications (less than 2 mm) has been tested in both tension and compression over a wide range of strain rates.

In this work, the room temperature tensile and compressive deformation behaviour of 1.6 mm thick magnesium alloy AZ31B rolled sheet material is characterized at different strain rates, from 10^{-3} to $10^{3}\,s^{-1}$. Compressive low and high strain rate tests were performed on adhesively bonded stacked sheet specimens which enabled in-plane compressive testing of sheet material by delaying buckling during testing. In order to determine the anisotropy of the mechanical properties of the investigated material, tensile and compressive tests were performed in the rolling and TDs and at 45° to the RD (designated herein as RD, TD and 45°, respectively). Compressive tests were also performed in the through-thickness or normal direction (ND). The primary objective in this work is to characterize the anisotropy and tension–compression asymmetry in this hcp sheet alloy, and how this behaviour is altered by changes in the strain rate. In addition, the strong coupling between mechanical response and the initial crystallographic texture is identified and discussed in the light of deformation mechanisms known to operate at different orientations and strain rates. A new constitutive model to account for strain rate dependency under compressive loading is proposed to fit to the measured sigmoidal compressive flow response over a wide range of strain rates. In addition, the Zerilli–Armstrong hcp model is used to fit to the measured tensile response over the range of strain rate considered.

2. Experimental methods

(a) Material

A rolled commercial magnesium alloy sheet, AZ31B (3.0% Al, 1.1% Zn and 0.49% Mn) in the *fully annealed* condition (O-temper) was used in this study. The nominal thickness of the sheet is 1.6 mm, and the pole figure of initial texture is shown in figure 1. EBSD data were obtained using a LEO 1450 scanning electron microscope fitted with a TSL EBSD camera. The EBSD data were analysed using the TSL OIM software (ver. 4.6). The data were cleaned to remove bad data points, and only data points having a confidence index above 0.2 were retained for the analyses. From the pole figures presented in figure 1, the AZ31B sheet exhibits a strong basal plane pole figure, with a minor spreading in the RD and strong peak intensity. The data indicate that the majority of grains are oriented with their crystallographic *c*-axes along the sheet ND, with some grains tilted towards the sheet RD.

(b) Specimen preparation and mechanical testing

The uniaxial tensile experiments used a miniature dog-bone specimen developed by Smerd *et al.* [20] and shown in figure 2*a*. This geometry has a gauge length of 12.5 mm and 1.75 mm width, which is small enough to minimize signal rise time and achieve dynamic equilibrium during high-rate experiments up to a strain rate of $1000\,s^{-1}$. Furthermore, this specimen geometry has been shown to produce stress–strain data matched to that of ASTM tensile specimens (E 8M-04) up to the ultimate tensile stress (UTS) for a range of materials [15,21]. This correlation is acceptable, because the flow stress up to UTS is of primary importance in constitutive fitting.

In-plane compression testing of Mg alloy sheet is required to characterize the asymmetric material behaviour at the desired orientations. In this work, for compression testing, adhesively bonded sheet laminates, as shown in figure 2*b*, were prepared in order to overcome any buckling during testing [9,22]. A high performance structural adhesive material, Master Bond Supreme 10HT, was used to bond the sheets into cubes which could be tested over a wide range of strain rates. To improve the performance of the adhesive, the bonding surface of each sheet was

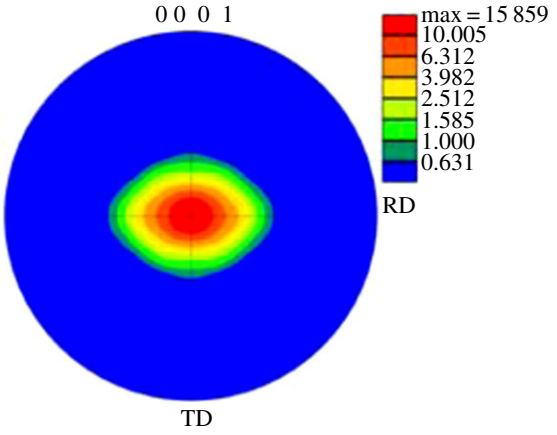

Figure 1. Pole figure of initial texture of AZ31B rolled sheet. (Online version in colour.)

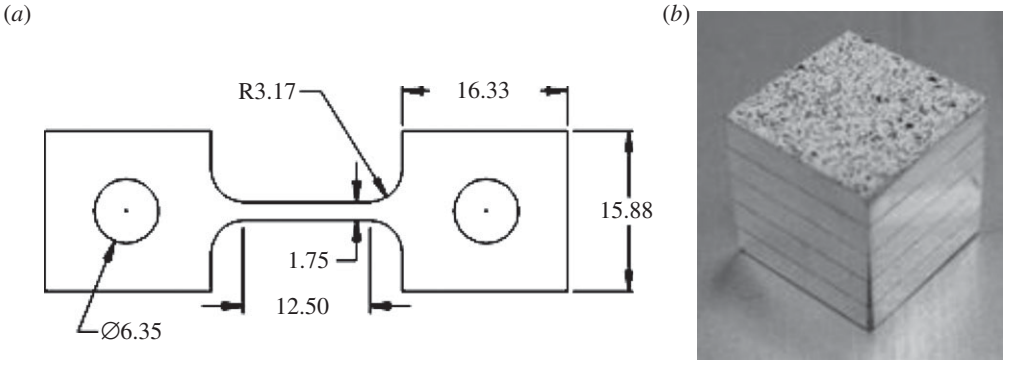

Figure 2. Tensile and compression samples used in this work, (*a*) miniature dog-bone sample; (*b*) stacked sheet sample ($8 \times 8 \times 8$ mm).

roughened by light machining. While testing, an oil-based lubricant, Krytox- (perfluoropolyether-based oil with polytetrafluoroethylene powder), was used to reduce the friction between the contacting faces of the tested sample and the apparatus. The effects of sample size, different adhesives used for stacking and different lubrication conditions between interfaces were studied and presented elsewhere [9]. Care was taken to confirm that the specimens deform in a uniform manner until the onset of necking or buckling instability beyond which the data were discarded. In order to have further confidence in the stacked specimens used to characterize the compressive response of sheet material, Ghaffari Tari *et al.* [23] compared the compressive response of a 6 mm thick monolithic sheet, having a crystallographic texture that was similar to that of the sheet material used in this work, and found similar stress–strain response, with earlier failure in the stacked samples.

Quasi-static ($0.001\,s^{-1}$ to $0.1\,s^{-1}$) tensile tests were performed using a servo-hydraulic Instron machine. Specimen elongation was measured using a 12.5 mm gauge length extensometer. Intermediate strain rate ($1\,s^{-1}$ to $100\,s^{-1}$) tensile experiments were performed using a hydraulic intermediate strain rate apparatus. An enhanced laser displacement system was used to measure the specimen elongation. High strain rate tensile tests at nominal strain rates of 500 and $1000\,s^{-1}$ were performed using the tensile split Hopkinson bar apparatus, and strain gauges mounted on the incident and transmission bar were used to measure the specimen elongation. Low rate uniaxial compression testing was performed using customized grips for Instron apparatus. The strain measurement was performed using a digital image correlation system. The high

strain rate compression experiments were conducted using the compressive split Hopkinson bar apparatus. A comprehensive description of the apparatus and the techniques used to calculate the engineering stress and strain data can be found elsewhere [11,20,21].

3. Experimental results and discussion

(a) Effect of the strain rate on constitutive response

The influence of strain rate on the tensile flow behaviour of AZ31B-O alloy sheet can be seen in figure 3 in which the true stress versus effective plastic strain response for each strain rate are plotted for the RD, TD and 45° orientation. For each strain rate, at least three successful tests were performed. The reproducibility of the ultimate tensile strength was better than 4 MPa for the tests performed at strain rates below $100\,s^{-1}$ and 14 MPa for the tests performed at 500 and $1000\,s^{-1}$. The average response is determined by interpolating the flow stress at plastic strain increments of 0.002 and then averaging the stress level at corresponding strains. The flow curves corresponding to the tensile tests exhibit a concave downwards shape, owing to the predominant operation of crystallographic slip at all strain rates. It is observed that the tensile specimens failed without any necking in the thickness and width directions at all strain rates and orientations.

The data presented in figure 3 demonstrate that there is a clear increase in tensile strength as the strain rate increases in all the three directions, i.e. the material shows positive strain rate sensitivity in all the orientations tested. This behaviour can mainly be attributed to the strain rate dependency of the critical resolve shear stress (CRSS) of non-basal slip systems [4,8]. Over the entire range of strain rates considered, the yield stress along the TD is higher than that obtained along the RD, similar to the results reported by Agnew & Duygulu [4] and Khan *et al.* [7]. Indeed, the flow curves in the RD show a stress increase of approximately 50 versus 70 MPa for the flow curves in the TD. The lower yield stress in the RD is related to the slight spread of the basal fibres towards the RD in the initial material, which allows relatively easier activation of basal slip by tensile loading along the RD [4,8].

The curves presented in figure 4 illustrate the measured true stress versus effective plastic strain response from uniaxial compression tests carried out at quasi-static and dynamic strain rates until failure along the RD TD, 45° and ND. The curves plotted correspond to the average response from a minimum of three experiments at each strain rate. The repeatability of the flow stress at a given strain was typically better than 10 MPa, depending upon the strain rate, and the average response is determined by interpolating the flow stress at plastic strain increments of 0.002 and then averaging the stress level at corresponding strains. From figure 4*a–c*, it is observed that the shape of the stress–strain curves is concave upwards (S-shape) for the in-plane compressive loading at all strain rates. Such a stress–strain response is consistent with the predominance of [10–12] twinning that takes place during the first stages of deformation, leading to an 86° rotation of the *c*-axes (which are perpendicular to compression axis in most grains before deformation) which brings them into alignment with the compression axis. This initial twinning is followed by strong strain-hardening behaviour at larger strains owing to the subsequent operation of non-basal slip [4,7,8]. It is observed from figure 4*d* that the compressive yield and flow stresses are much higher in through-thickness compression (ND) when compared with in-plane compressive loading. The through-thickness compression curve shows a concave downwards shape owing to the predominance of pyramidal slip deformation, which is consistent with trends reported by earlier studies [4–8]. The through-thickness compression curve shows similar hardening characteristics as in-plane tension (figure 3), but has higher stress values for the same strain. The failure strains for the ND specimens are smaller than for the corresponding in-plane compression or tension experiments.

When assessing the effect of strain rate on the in-plane compressive response, the flow stress in the twinning regime (strains less than 4%) is strain rate independent, whereas in the subsequent crystallographic slip regime (strains greater than 4%), the flow stress response shows strong strain rate sensitivity in all in-plane loading directions (figure 4). The through-thickness tests exhibit

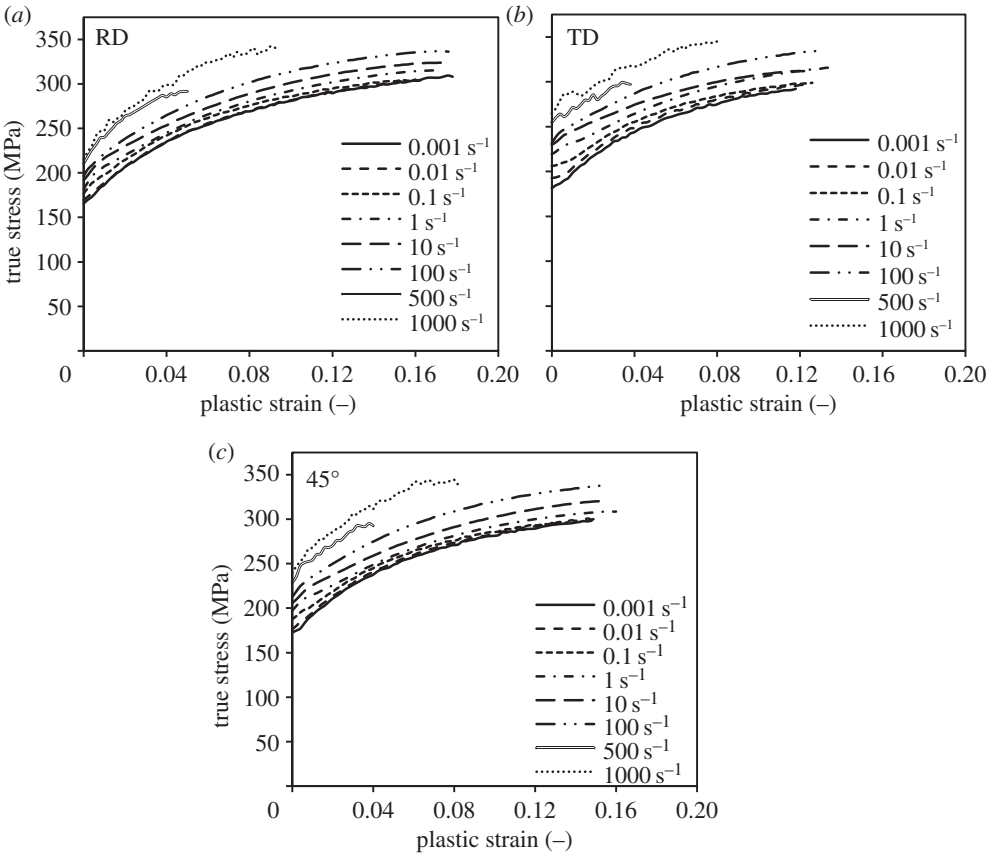

Figure 3. Effect of strain rate on the tensile flow curves of AZ31B-O Mg alloy sheet in different orientations and strain rates.

very mild strain rate sensitivity in terms of the initial yield strength, but the work hardening rate increases for higher rates of loading.

(b) Effect of strain rate on anisotropy and tension–compression asymmetry

The investigated AZ31B sheet exhibits moderate in-plane anisotropy which does not appear to be affected significantly by changes in the strain rate. The dependency of the tensile stress–strain response on strain rate and load orientation can be seen in figure 5*a*, which illustrates the tensile flow curves for AZ31B sheet in the RD, TD and 45° orientation at strain rates of 0.1, 100 and 1000 s^{-1}. All three orientations show a consistent ranking of strength, with the highest strength in the TD and lowest strength in the RD. The material exhibits a strong increase in flow stress with strain rate; for example, the flow stress at 6% plastic strain along the RD increases by 50 MPa for an increase in the strain rate from 10^{-1} to 10^{3} s^{-1}. Similar increases are observed in the TD and 45° orientation. Figure 5*b* shows the compressive flow curves in the RD, TD and 45° orientation at strain rates of 0.01 and 1000 s^{-1}. The material exhibits strain rate-independent flow stress in the twinning regime and shows strong strain rate effect in the slip-dominated regime. However, the effect of sheet orientation is clearly negligible in both the twinning and slip-dominated regimes of the compressive stress–strain response.

While the level of in-plane anisotropy observed in the stress–strain response is relatively mild, there are high levels of anisotropy exhibited in terms of the *r*-values or Lankford coefficients measured along the three material orientations tested. The *r*-value (instantaneous value) is defined as the ratio of width strain rate to thickness strain rate during uniaxial testing. The evolution of instantaneous *r*-values measured at room temperature along different orientations

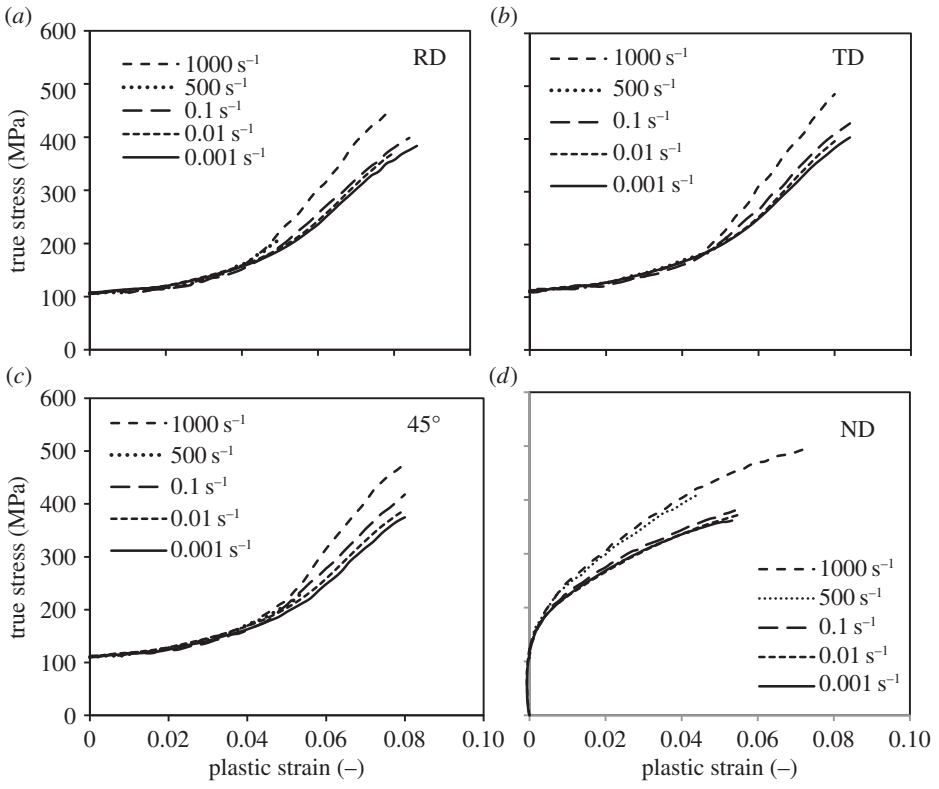

Figure 4. Effect of strain rate on the compression flow curves of AZ31B-O Mg alloy sheet in different orientations and strain rates.

under both tensile and compressive loading at a strain rate of $0.01\,s^{-1}$ is plotted in figure 5*c*. In general, a Lankford coefficient of unity indicates an isotropic response. The measured *r*-values in figure 5*c* are dramatically different from unity and reflect the strong difference in resistance to in-plane versus through-thickness deformation. This behaviour can be traced to the strong basal texture seen in figure 1. There is also strong variation in the *r*-values measured along the different sheet orientations which is indicative of a higher degree of in-plane anisotropy than that observed based solely upon the variation in stresses seen in figure 5*a* (tension) and figure 5*b* (compression). These in-plane variations are attributed to the differences in spreading of the basal texture between the TD and RD directions seen in figure 1. The effect of strain rate on *r*-value was not measured in this research; however, Ghaffari Tari & Worswick [24] found that tensile *r*-values for this alloy were rate-insensitive at room temperature in the strain rate regime 0.001 to $1.0\,s^{-1}$. They also determined that the rate sensitivity increased at elevated temperatures. Khan *et al.* [7] also studied the strain rate sensitivity of AZ31B sheet at elevated temperatures and found that the material exhibits positive strain rate sensitivity at all temperatures, strain rates and directions in both tension and compression.

Figure 6*a* serves to illustrate the tension–compression asymmetry of this alloy. The measured true stress versus effective plastic strain for in-plane tension and compression at a strain rate of $0.001\,s^{-1}$ along the RD and TD is plotted. Data are also plotted for through-thickness compressive loading. It is observed that the yield stress for in-plane compression loading is approximately one-half of the yield stresses in tension (figure 6*a*). The in-plane compression curves exhibit a sigmoidal upwards shape. The initial plateau results from extension twinning which saturates at higher strain values, leading to subsequent large strain-hardening rates and weaker contraction twinning effects [4,7,8]. The in-plane tensile flow curves and ND compression samples exhibit characteristics of crystallographic slip-dominated deformation [2,7,8]. The level of in-plane anisotropy in the measured stresses remains consistent in tension versus compression with a

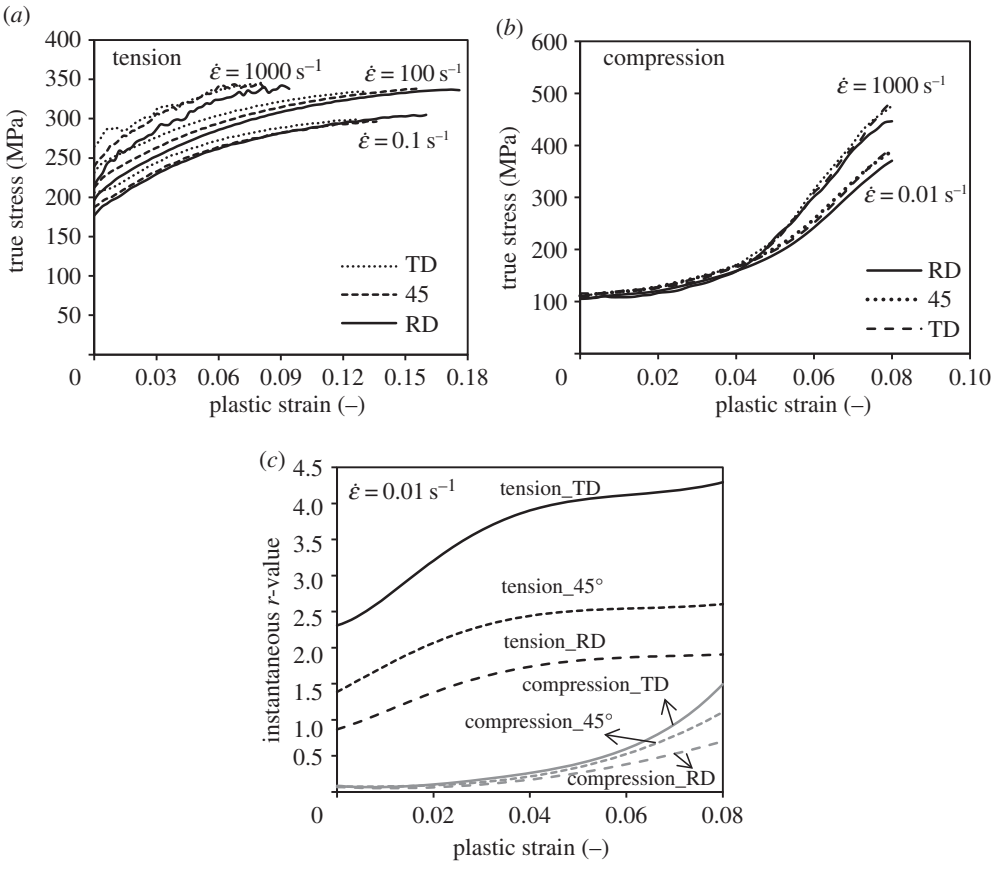

Figure 5. Effect of sheet orientation on (*a*) tensile, (*b*) compressive flow curves and (*c*) evolution of instantaneous *r*-values in tensile and compressive loading of AZ31B-O Mg alloy sheet at different strain rates.

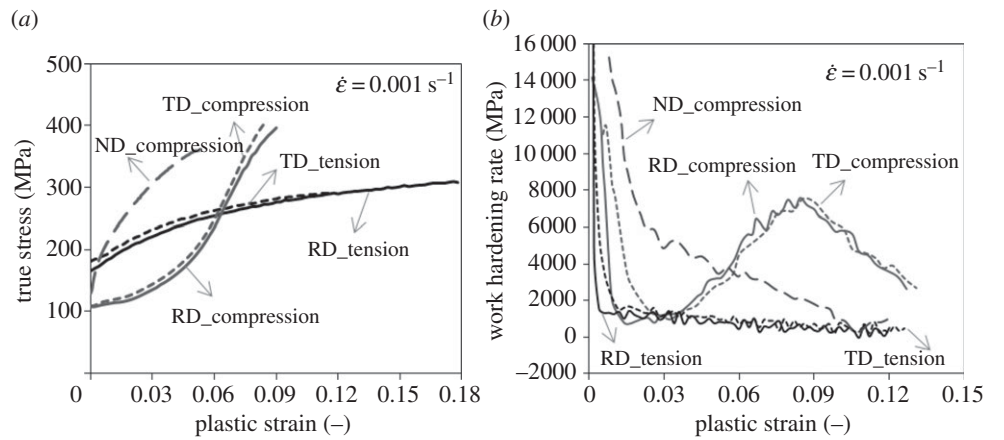

Figure 6. Tension–compression asymmetry of (*a*) flow curves, (*b*) their corresponding work hardening rates in different orientations.

mildly lower stress level for a given strain in the RD compared with the TD. The very high stress level in the ND compression samples is attributed the alignment of the loading axis with the sheet ND. Basal slip and extension twinning, with their low CRSS requirements, are not activated for this loading case, requiring non-basal slip processes to be activated, with their associated higher CRSS levels [7,8].

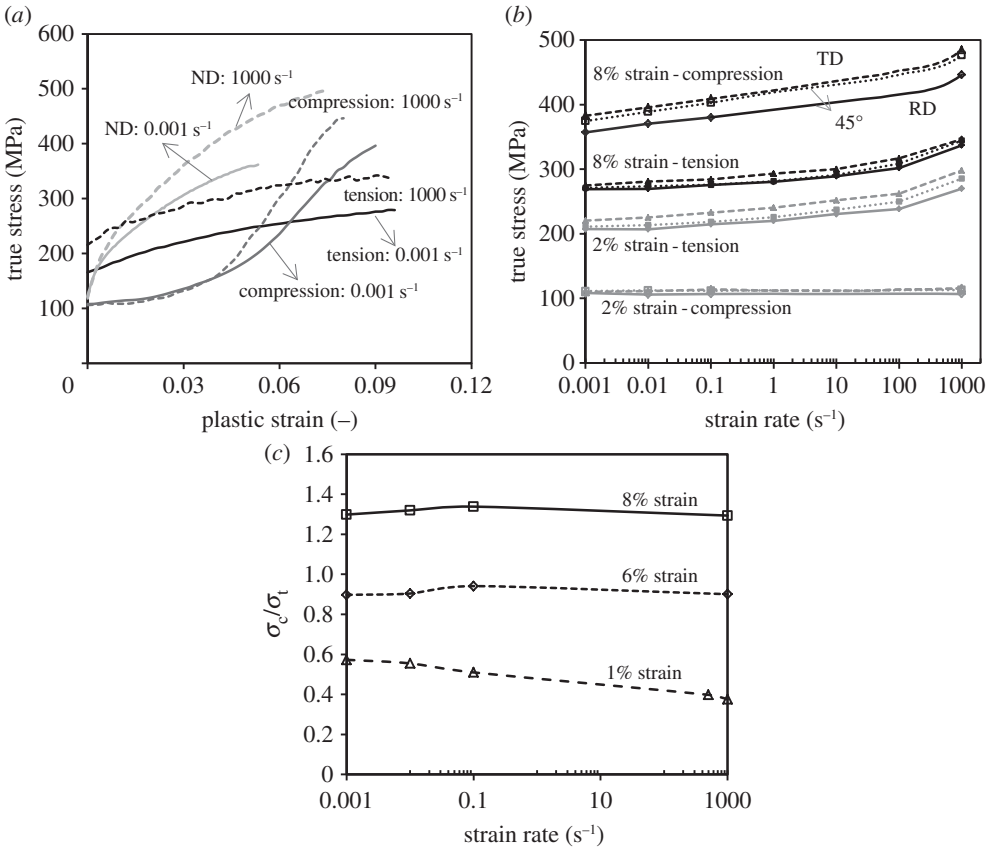

Figure 7. Effect of strain rate on tension–compression asymmetry (*a*) true stress versus effective plastic strain, (*b*) true stress versus strain rate (note that no experimental compressive data is available at strain rates 1, 10 and 100 s^{-1} and the plotted trend lines correspond to equation (4.3)) and (*c*) compression–tension ratio at different plastic strains versus strain rate.

Figure 6*b* shows the variation of work hardening rate corresponding to the flow curves presented in figure 6*a* for the tension, in-plane compression tests in the RD and TD and the through-thickness (ND) tests. The hardening rate in the compression tests in both the RD and TD first drops, corresponding to the twinning regime, but then increases, as slip becomes dominant, before falling off again. The peak hardening rate corresponds to about 9% strain where the stress–strain curves of the compression tests in the RD and TD shown in figure 6*b* exhibit rapid hardening, corresponding to saturation of twinning and activation of crystallographic slip. The variation of hardening rates in tensile samples and through-thickness compression samples shows a monotonic decrease with strain. But, the rate of work hardening for through-thickness tests is higher than the work hardening rate of the tensile tests in the RD and TD, which is consistent with the available deformation mechanisms for through-thickness compression discussed above.

Figure 7*a* shows the true stress versus effective plastic strain response for in-plane tension and compression along the RD as well as for ND compression. The data are shown for two strain rates (10^{-3} and 10^{3} s^{-1}), and illustrate how an increase in the strain rate affects the tension–compression asymmetry. It can be seen that the twinning-dominated deformation at low strains under in-plane compression is strain rate insensitive, whereas the slip-dominated processes are strain rate sensitive. The rate sensitivity under various loading directions and orientations is further explored in figure 7*b*, in which true stress as a function of strain rate (logarithmic scale) is plotted. The data are plotted for strain levels of 2% and 8% plastic strain. At low strains (2%), the in-plane

compressive response is twinning-dominated and strain rate-insensitive, as indicated by the low slope. At higher strains (8%), the compressive rate sensitivity is strong due to the activation of slip and is comparable with the tensile rate sensitivity which is also slip dominated. From figure 7*b*, it can be seen that the degree of tension–compression asymmetry will increase with strain rate, primarily at lower strain levels. Figure 7*c* depicts the ratio of the flow stress in compression to that in tension as a function of strain rate at plastic strains of 1%, 6% and 8% along the RD. This figure serves to further illustrate how an increase in the strain rate influences the degree of compression–tension asymmetry. It is observed that at lower strain levels (1%), the degree of compression–tension asymmetry increases with increase in the strain rate. At lower strain levels, the in-plane compressive flow stress corresponds primarily to rate-insensitive twinning, whereas the tensile flow stress is due to rate-sensitive slip deformation leading to the strong strain rate dependency of the compression–tension ratio. On the other hand, at elevated strain levels, both compressive and tensile plastic occurs through slip, making the rate dependency of the compression–tension ratio.

4. Constitutive modelling

(a) A rate-sensitive constitutive equation for twinning-slip-dominated compressive response

For the slip-dominated concave downwards work hardening behaviour commonly observed in cubic materials, a wide variety of accurate phenomenological models exist in the literature that can capture the rate and temperature dependency with very good accuracy [25–29]. In this work, one of these models, the Zerilli–Armstrong hcp phenomenological model [29], is fit to the measured tensile behaviour, as presented below. Unfortunately, such rate-sensitive models do not account for the effects of deformation twinning on the plastic deformation of magnesium alloys, namely the sigmoidal stress–strain response (figure 4*a–c*) which leads to the very strong difference between the mechanical response in tension and compression.

In order to model the sigmoidal compressive hardening response commonly observed in hcp materials owing to twinning followed by slip-dominated deformation mechanisms, a limited number of phenomenological models are available in the published literature. Kim *et al.* [30] and Li *et al.* [31] used a Voce-type relation to model the sigmoidal compressive response. Yoon *et al.* [32] used the dose–response law [33] to describe the sigmoidal compressive flow response in the simulation of axial crushing of a tube. However, these models do not take rate sensitivity into account, in particular the rather novel behaviour identified in this work in which the twinning plateau does not appear to be rate-sensitive, whereas the subsequent slip-dominated response is. Here, a new phenomenological constitutive relation is proposed to capture the sigmoidal *rate-dependent* compressive response commonly observed in hcp materials. The model starts with the Morgan–Mercer–Flodin (MMF) equation [34], which was primarily developed for describing the nutritional response/growth in organisms faced with a limiting nutrient resource, and has the following form:

$$y_i = \alpha - \frac{\alpha - \beta}{(1 + (\kappa x_i)^{\delta})}, \tag{4.1}$$

where α is the value of upper asymptote, β is the value of y_i at $x_i = 0$, κ is the growth rate scaling parameter and δ is a parameter that controls the location of the point of inflection for the curve and defines the shape of the curve. Alternatively, when the upper asymptote, α is unknown, the MMF equation can be written

$$y_i = \frac{\kappa_1 \beta + \kappa_2 x_i^{\delta}}{(\kappa_2 + x_i^{\delta})}. \tag{4.2}$$

In this work, a new phenomenological constitutive relation is proposed based on the form of equation (4.2), to capture the sigmoidal *rate-sensitive* compressive flow response commonly

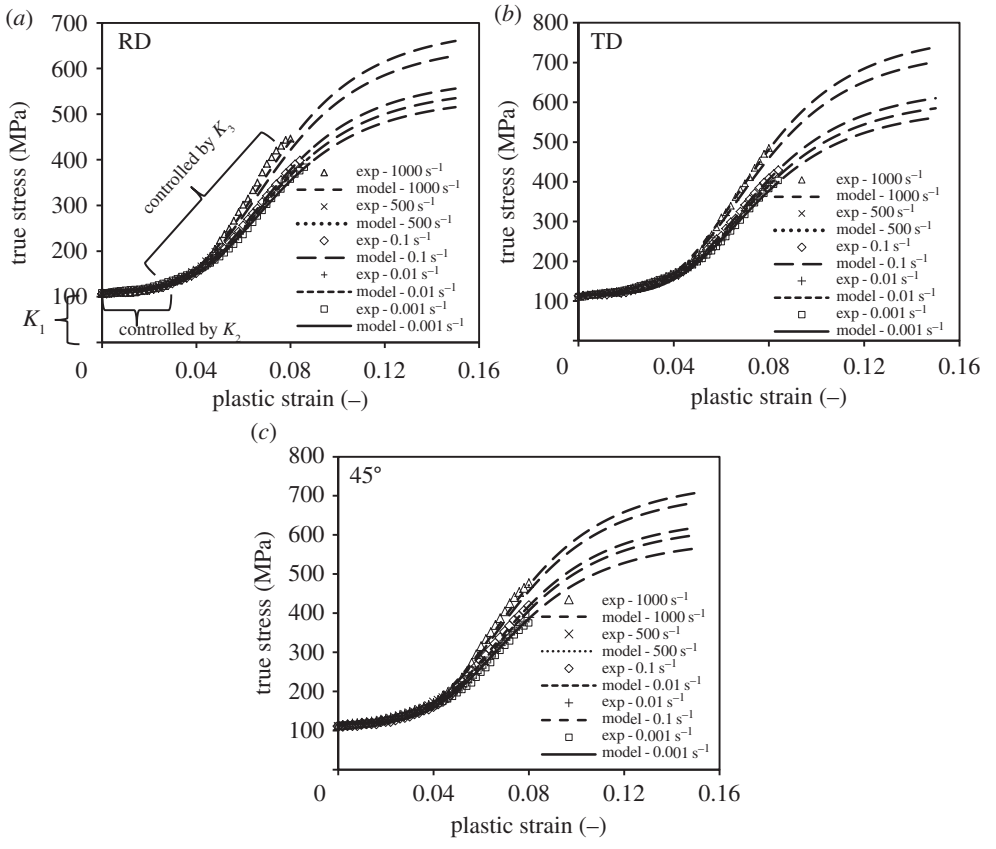

Figure 8. Compressive true stress–plastic strain curves in the RD, TD and 45°—experiments (symbols), proposed model (curves) and extrapolation (long-dashed curves) at different strain rates.

observed in hcp materials:

$$\sigma^C = \frac{[K_1 K_2 - (K_3 \bar{\varepsilon}_p^{K_4} / 1 - K_5 \exp(-K_6 \ln \dot{\varepsilon}_p))]}{K_2 + \bar{\varepsilon}_p^{K_4}}, \tag{4.3}$$

where σ^C is the equivalent stress, $\bar{\varepsilon}_p$ is the effective plastic strain, $\dot{\varepsilon}_p$ is the rate of effective plastic strain and K_1 is the initial yield strength. K_2 controls the extent of the plateau associated with the twinning regime, and K_3 is a scaling parameter that controls the slip-dominated region of the hardening curve. Parameter K_4 controls the point of inflection. Parameters K_5 and K_6 define the strain rate dependency of the flow curve, as shown in figure 8*a*. Note that equation (4.3) does not capture thermal softening effects and is strictly valid for isothermal cases. In this work, all of the experiments were performed at room temperature, and the temperature rise was estimated to be less than 68°C based on plastic work considerations. Ongoing research is addressing the incorporation of thermal softening into equation (4.3).

In order to assess the proposed constitutive equation, equation (4.3) was fit to the measured response, and a comparison between the measured and predicted response was carried out. It is noted that in the regression analysis, measured true stress versus plastic strain data at strain rates of 0.001, 0.01 and 1000 s^{-1} was used in the regression analysis. The measured data at strain rates of 0.1 and 500 s^{-1} were not used in the regression, but were used to assess the quality of the fit, as presented below. The measured data used in the regression analysis were limited to the plastic strain range for which (i) the strain rate was approximately constant; and (ii) the ultimate tensile strength or UTS had not yet been reached so as to avoid the onset of diffuse necking.

Table 1. Parameters of the proposed sigmoidal constitutive law for AZ31B sheet.

parameter	RD	45°	TD
K_1 (MPa)	114.2	119.4	117.5
K_2	5.3×10^{-5}	5.3×10^{-5}	5.6×10^{-5}
K_3	12.1	12.1	12.1
K_4	3.8	3.8	3.8
K_5	1.02	1.02	1.02
K_6	3.5×10^{-4}	2.5×10^{-4}	3.5×10^{-4}
correlation coefficient	0.99	0.99	0.99
mean absolute error (%)	4.0	4.0	4.0

For each test condition, the average curves presented in figure 4 were used. Each average curve represents three repetitions, interpolated at strain increments of 0.2%, thus ensuring that each experiment contributes equally to the constitutive fit. Separate regressions were performed for each material direction, and the resulting material parameters are found in table 1. The correlation coefficients exceed 0.995, and the mean absolute errors are around 4%, indicating good-quality fits to the compressive data.

The predicted flow curves for different strain rates, using the numerical values for the constitutive parameters K_1–K_6 for the RD, 45° and TD directions in table 1 are compared with the measured flow curves in figure 8. It can be observed that good agreement with the experimental results is obtained, especially in the TD and 45° orientations. It is also observed that good agreement is obtained between the predicted response at strain rates of 0.1 and 500 s^{-1}, and the corresponding measured data which were not used in the regression. For illustrative purposes, the extrapolation of the curves beyond the range of valid data in this work is shown as a dashed line. This extrapolation is shown solely to demonstrate that this constitutive equation is capable of capturing the inflection commonly observed in hcp metals; however, the reader is cautioned that the stress levels beyond the measured values have not been validated.

It is noted that the constitutive parameters in table 1 are almost identical for all material directions, with the exception of the initial yield parameter K_1. This outcome indicates that the work hardening response and strain rate sensitivity in all three material directions are quite similar and that the in-plane material anisotropy, in terms of strength, is manifest primarily in the differences in initial yield response. As mentioned above, the difference in strength level with material direction is relatively mild, although the *r*-values reflect a stronger degree of in-plane anisotropy.

(b) Constitutive fits to the tensile response

Zerilli & Armstrong [29] introduced a constitutive relation to model the strain rate- and temperature-dependent response of hcp metals, by combining the terms from their earlier bcc and fcc constitutive models [27,28]. In developing separate formulations for each crystal structure, Zerilli & Armstrong [27,28] concluded that overcoming Peierls–Nabarro barriers, associated with dislocation motion, was the principal thermal activation mechanism for bcc metals, whereas dislocation interactions, and thus density, were the controlling mechanism for fcc metals. They considered hcp constitutive behaviour to combine aspects of both bcc and fcc strain rate sensitivity. The hcp version of the Zerilli–Armstrong [29] constitutive model is given by

$$\bar{\sigma} = C_0 + \left(C_1 + C_2\sqrt{\bar{\varepsilon}_p}\right)\exp[(-C_3 + C_4 \ln(\dot{\varepsilon}_p))T] + C_5\bar{\varepsilon}_p^n, \tag{4.4}$$

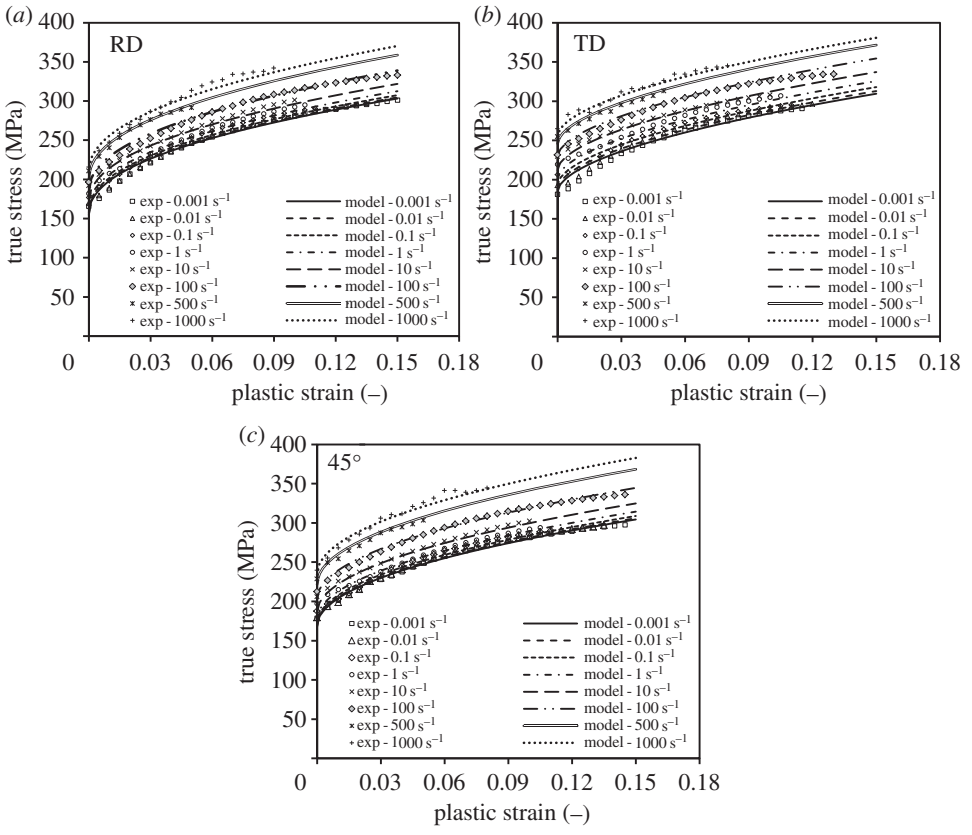

Figure 9. Tensile true stress–plastic strain curves in the RD, TD and 45°—experiments (symbols) and Zerilli–Armstrong [29] model (curves) at different strain rates.

Table 2. Parameters of the Zerilli–Armstrong model for AZ31B sheet in three directions.

parameter	RD	45°	TD
C_0 (MPa)	152.7	166.1	177.6
C_1 (MPa)	28.7	10.6	30.4
C_2 (MPa)	17.6	5.1	0.4
C_3 (1/K)	3.9×10^{-3}	2.6×10^{-4}	1.0×10^{-3}
C_4 (1/K)	8.9×10^{-4}	9.4×10^{-4}	6.0×10^{-4}
C_5 (MPa)	349.4	344.8	354.1
n	0.4	0.5	0.5
correlation coefficient	0.98	0.98	0.98
mean absolute error (%)	4.0	4.0	4.0

where $\bar{\varepsilon}_p$ is the effective plastic strain, $\dot{\varepsilon}_p$ is the rate of effective plastic strain and T is the absolute temperature. C_0, C_1, C_2, C_3, C_4, C_5 and n are the material constants which are determined from the experimental data. The current AZ31B alloy does, in fact, exhibit such a combination of 'bcc' and 'fcc response', that is, a rate-dependent initial yield strength commonly observed in bcc alloys, and a rate-dependent work hardening commonly observed in fcc alloys. In equation (4.4), a bcc-like response is represented by material parameters C_1, C_3 and C_4 which introduce the

dependency of yield strength on strain rate and temperature, whereas C_5 and n represent the rate- and temperature-independent work hardening typical of bcc material behaviour. To introduce fcc-like material behaviour, parameter C_0 represents a rate-insensitive yield strength, whereas parameters C_2 and C_4 introduce strain-rate-dependent work hardening.

The constitutive parameters required by the Zerilli–Armstrong model (equation (4.4)) were fit to the experimental results using a nonlinear regression algorithm. The measured true stress–plastic strain data at strain rates of 0.001, 0.01, 1, 10 and 1000 s^{-1} was used in the regression analysis. It is noted that in the nonlinear regression procedure, all of the parameters were unconstrained and simultaneously fit with the experimental data for a given orientation. In table 2, the estimated parameters of the Zerilli–Armstrong hcp model are given for the RD, TD and 45° directions, and the corresponding predicted flow curves for different strain rates are compared with the measured flow curves in figure 9. It can be observed that good agreement with experimental results is obtained in three directions. Note that as part of the validation process, data for strain rates of 0.1, 100 and 500 s^{-1} were not considered in the regression, and the predicted response using the calibrated material coefficients is observed to agree well with the measured data at these strain rates. The correlation coefficient and the mean absolute error for all three fits are given in table 2. The correlation coefficients all exceeded 0.989, and the mean absolute error was around 4.0%, both demonstrating that the fits are of high quality.

The constitutive relations described above can be incorporated into numerical models to simulate deformation of AZ31 sheets that encounter different strain paths during industrial processing and need different constitutive relations depending on the stress state to describe the material behaviour accurately.

5. Conclusion

1. Slip- versus twin-dominated deformation within AZ31B exhibits rather different strain rate sensitivity, slip processes being strongly rate sensitive, whereas twinning deformation appearing rate insensitive. The actual rate sensitivity becomes a function of the as-received texture and the orientation and sign (tension versus compression) of the applied loading. Thus, tensile in-plane loading is rate-sensitive, whereas compressive in-plane loading is initially rate-insensitive until twinning is exhausted after which slip processes are activated with associated rate sensitivity.
2. The level of in-plane anisotropy within the AZ31B tested in this research is not significantly affected by strain rate.
3. The new constitutive model proposed herein is shown to accurately capture the sigmoidal compressive flow stress response associated with twinning followed by slip-dominated hardening over a range of strain rates. The reader is cautioned that the fits are not validated beyond the measured strain levels.
4. The Zerilli–Armstrong [29] hcp constitutive model is shown to accurately capture the in-plane tensile response of the current AZ31B sheet over the range of strain rates considered.

Acknowledgement. This research was carried out under the framework of the Research Programme of the Magnesium Network (MagNET), Canada. The authors thank Dr Alex Bardelcik of the University of Waterloo for helpful discussions on various material characterization techniques.

Funding statement. Financial support from General Motors of Canada, MagNET, Automotive Partnership Canada, the Natural Sciences and Engineering Research Council of Canada, the Canada Research Chairs Secretariat and the Ontario Research Fund is gratefully acknowledged.

References

1. Carter JT, Melo AR, Savic V, Hector LG, Krajewski PE. 2011 Structural evaluation of an experimental aluminum/magnesium decklid. SAE Paper no. 2011-01-0075.

2. Min J, Cao Y, Carter JT, Verma R. 2012 *Comparison of tensile properties and crystallographic texture of three magnesium alloy sheets*. London, UK: John Wiley & Sons, Inc.
3. Barnett MR. 2003 A Taylor model based description of the proof stress of magnesium AZ31 during hot working. *Metall. Mater. Trans. A* **34**, 1799–1806. (doi:10.1007/s11661-003-0146-5)
4. Agnew SR, Duygulu O. 2005 Plastic anisotropy and the role of non-basal slip in magnesium alloy AZ31B. *Int. J. Plast.* **21**, 1161–1193. (doi:10.1016/j.ijplas.2004.05.018)
5. Bohlen J, Nürnberg MR, Senn JW, Letzig D, Agnew SR. 2007 The texture and anisotropy of magnesium-zinc rare earth alloy sheets. *Acta Mater.* **55**, 2101–2112. (doi:10.1016/j.actamat.2006.11.013)
6. Hilditch T, Atwell D, Easton M, Barnett M. 2009 Performance of wrought aluminum and magnesium alloy tubes in three-point bending. *Mater. Des.* **30**, 2316–2322. (doi:10.1016/j.matdes.2008.11.020)
7. Khan AS, Pandey A, Gnäupel-Herold T, Mishra RK. 2011 Mechanical response and texture evolution of AZ31 alloy at large strains for different strain rates and temperatures. *Int. J. Plast.* **27**, 688–706. (doi:10.1016/j.ijplas.2010.08.009)
8. Ulacia I, Dudamell N, Gálvez F, Yi S, Pérez-Prado M, Hurtado I. 2010 Mechanical behavior and microstructural evolution of a Mg AZ31 sheet at dynamic strain rates. *Acta Mater.* **58**, 2988–2998. (doi:10.1016/j.actamat.2010.01.029)
9. Kurukuri S, Ghaffari Tari D, Worswick MJ, Carter JT, Mishra RK. 2012 Dynamic characterization of AZ31B and ZEK100 magnesium alloy sheets. In *Int. Conf. Mag. Alloys and Applications*. Vancouver, BC, Canada.
10. Kurukuri S, Bardelcik A, Worswick MJ, Mishra RK, Carter JT. 2012 High strain rate characterization of ZEK100 magnesium rolled alloy sheet. *EPJ Web Conf.* **26**, 01042. (doi:10.1051/epjconf/20122601042)
11. Kurukuri S, Worswick MJ, Bardelcik A, Carter JT, Mishra RK. Submitted. Constitutive behavior of commercial grade ZEK100 magnesium alloy sheet over wide range of strain rates. *Metall. Mater. Trans. A*.
12. Lou XY, Li M, Boger RK, Agnew SR, Wagoner RH. 2007 Hardening evolution of AZ31B Mg sheet. *Int. J. Plast.* **23**, 44–86. (doi:10.1016/j.ijplas.2006.03.005)
13. Ghaffari Tari D, Worswick MJ, Winkler S. 2013 Experimental studies of deep drawing of AZ31B magnesium alloy sheet under various thermal conditions. *J. Mater. Process. Technol.* **213**, 1337–1347. (doi:10.1016/j.jmatprotec.2013.01.028)
14. Ghaffari Tari D, Worswick MJ, Ali U, Gharghouri M. 2014 Mechanical response of AZ31B magnesium alloy experimental characterization and constitutive modeling considering proportional loading. *Int. J. Plast.* **55**, 247–267.
15. Hasenpouth D. 2010 Tensile high strain rate behavior of AZ31B magnesium alloy sheet. Master's thesis, University of Waterloo, Waterloo, ON, Canada.
16. Ulacia I, Salisbury CP, Hurtado I, Worswick MJ. 2011 Tensile characterization and constitutive modeling of AZ31B magnesium alloy sheet over wide range of strain rates and temperatures. *J. Mater. Process. Technol.* **211**, 830–839. (doi:10.1016/j.jmatprotec.2010.09.010)
17. Mukai T, Yamanoi M, Higashi K. 2000 Ductility enhancement in magnesium alloys under dynamic loading. *Mater. Sci. Forum* **350**, 97–104. (doi:10.4028/www.scientific.net/MSF.350-351.97)
18. El-Magd E, Abouridouane M. 2003 Influence of strain rate and temperature on the compressive ductility of Al, Mg and Ti alloys. *J. Phys.* **110**, 15–20.
19. Tucker MT, Horstemeyer MF, Gullett PM, El Kadiri H, Whittington WR. 2009 Anisotropic effects on the strain rate dependence of a wrought magnesium alloy. *Script. Mater.* **60**, 182–185. (doi:10.1016/j.scriptamat.2008.10.011)
20. Smerd R, Winkler S, Salisbury C, Worswick M, Lloyd D, Finn M. 2005 High strain rate tensile testing of automotive aluminum alloy sheet. *Int. J. Impact Eng.* **32**, 541–560. (doi:10.1016/j.ijimpeng.2005.04.013)
21. Thompson AC, Salisbury CP, Worswick MJ, Mayer R. 2006 Constitutive modeling of dual phase steel sheet and tube. *J. Phys.* **134**, 281–286.
22. Maeda Y *et al.* 1998 Experimental analysis of aluminum yield surface for binary Al-Mg alloy sheet samples. *Int. J. Plast.* **14**, 301–318. (doi:10.1016/S0749-6419(97)00065-X)
23. Ghaffari Tari D, Worswick MJ, Gharghouri M. 2013 Warm forming modeling of magnesium alloys using an evolving yield locus formulation.

24. Ghaffari Tari D, Worswick MJ. 2011 Experimental investigation of anisotropy evolution of AZ31 magnesium alloy sheets under tensile loading. *AIP Conf. Proc.* **1353**, 1547–1552. (doi:10.1063/1.3589737)
25. Voce E. 1948 The relation between stress and strain for homogeneous deformation. *J. Inst. Metals* **74**, 537–562.
26. Johnson G, Cook W. 1983 A constitutive model and data for metals subjected to large strains, high strain rates and high temperatures. *Proc. 7th Int. Symp. Ballistics*, pp. 541–547.
27. Zerilli FJ, Armstrong RW. 1987 Dislocation-mechanics-based constitutive relations for material dynamics calculations. *J. Appl. Phys.* **61**, 1816–1825. (doi:10.1063/1.338024)
28. Zerilli FJ, Armstrong RW. 1992 The effect of dislocation drag on the stress–strain behavior of fcc metals. *Acta Metall. Mater.* **40**, 1803–1808. (doi:10.1016/0956-7151(92)90166-C)
29. Zerilli FJ, Armstrong RW. 1995 Constitutive equation for hcp metals and high strength alloy steel. *ASME J.* **48**, 121–126.
30. Kim J, Ryou H, Kim D, Kim D, Lee W, Hong SH, Chung K. 2008 Constitutive law for AZ31B Mg alloy sheets and finite element simulation for three-point bending. *Int. J. Mech. Sci.* **50**, 1510–1518. (doi:10.1016/j.ijmecsci.2008.08.004)
31. Li M, Lou XY, Kim JH, Wagoner RH. 2010 An efficient constitutive model for room-temperature, low-rate plasticity of annealed Mg AZ31B sheet. *Int. J. Plast.* **26**, 820–858. (doi:10.1016/j.ijplas.2009.11.001)
32. Yoon J, Cazacu O, Mishra RK. 2013 Constitutive modeling of AZ31 sheet alloy with application to axial crushing. *Mater. Sci. Eng. A* **565**, 203–212. (doi:10.1016/j.msea.2012.12.054)
33. Motulsky H, Christopoulos A. 2004 *Fitting models to biological data using linear and nonlinear regression: a practical guide to curve fitting*. Oxford, UK: Oxford University Press.
34. Morgan PH, Mercer LP, Flodin NW. 1975 General model for nutritional responses of higher organisms. *Proc. Natl Acad. Sci. USA* **72**, 4327–4331. (doi:10.1073/pnas.72.11.4327)